NANO LETTERS

pubs.acs.org/NanoLett Letter

Stiff Shape Memory Polymers for High-Resolution Reconfigurable Nanophotonics

Wang Zhang, Hao Wang,* Alvin T. L. Tan, Anupama Sargur Ranganath, Biao Zhang, Hongtao Wang, John You En Chan, Qifeng Ruan, Hailong Liu, Son Tung Ha, Dong Wang, Venkat K. Ravikumar, Hong Yee Low, and Joel K. W. Yang*

Cite This: https://doi.org/10.1021/acs.nanolett.2c03007 Read Online

ACCESS | Metrics & More | Article Recommendations | Supporting Information

ABSTRACT: Reconfigurable metamaterials require constituent nanostructures to demonstrate switching of shapes with external stimuli. Yet, a longstanding challenge is in overcoming stiction caused by van der Waals forces in the deformed configuration, which impedes shape recovery. Here, we introduce stiff shape memory polymers. This designer material has a storage modulus of ~5.2 GPa at room temperature and ~90 MPa in the rubbery state at 150 °C, 1 order of magnitude higher than those in previous reports. Nanopillars with diameters of ~400 nm and an aspect ratio as high as ~10 were printed by two-photon lithography. Experimentally, we observe shape recovery as collapsed and touching structures overcome stiction to stand back up. We develop a theoretical model to explain the recoverability of these sub-micrometer structures. Reconfigurable structural color prints with a resolution of 21150 dots per inch and holograms are demonstrated, indicating potential applications of the stiff shape memory polymers in high-resolution reconfigurable nanophotonics.

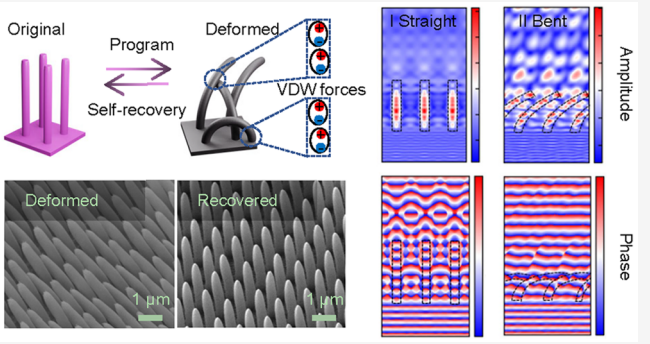

KEYWORDS: *reconfigurable structures, two-photon lithography, sub-micrometer 3D printing, van der Waals forces, nanophotonics*

Compliant and reconfigurable structures are used in areas such as biological engineering,[1,2] soft robotics,[3−5] and flexible electronics.[6,7] At the macroscale, configuration transformation is feasible through the exposure of stimuli-responsive materials to heat,[8−10] water,[11,12] light,[13−15] electricity,[16] and magnetic fields.[17,18] Pushing these reconfigurable structures to the sub-micrometer scale would enable new applications in nanophotonics,[19] sensors,[20,21] and microrobotics.[22] However, a longstanding challenge in reconfigurable nanostructures is related to their significantly higher surface-to-volume ratio where van der Waals (VDW) forces[23] dominate. As VDW forces exceed the internal restoring forces as structures decrease in size, nanostructures that come in physical contact tend to remain "stuck" and never detach.[24−26]

A common approach to avoid permanent deformation is to increase the restoring forces. For instance, the restoring force can be increased using interconnected geometries.[27] Different stimuli-responsive materials have been fabricated based on this strategy.[28−31] However, these interconnected structures will reduce the resolution and lead to severe cross-talk between pixels,[32] weakening the performance in fields requiring high resolution such as nanophotonics, where isolated pixels[33,34] are preferred. Increasing the restoring forces in isolated elements requires a higher material stiffness. Unfortunately, existing stimuli-responsive materials for reconfigurable devices at the macro to micro scale have low storage moduli ranging from approximately kPa to less than ~10 MPa[8] in the rubbery state. There is a lack of high modulus materials to pattern reconfigurable structures at the sub-micrometer scale. Hence, new materials are needed with sufficient flexibility to be deformed and collapse when set yet possess a strong capacity for recovery to overcome the influence of VDW forces and detach during the reset phase. Simultaneously, suitable fabrication methods need to be developed to explore new applications of stimuli-responsive materials at the sub-micrometer scale.

In this work, we introduce stiff shape memory polymers for high-resolution reconfigurable nanophotonics. We formulated acrylic acid based shape memory polymers (SMPs) and developed a resin for two-photon polymerization lithography (TPL). We fabricated nanopillars with an ~400 nm diameter and an aspect ratio of ~10 by TPL. With the material developed,

Received: July 29, 2022
Revised: November 7, 2022

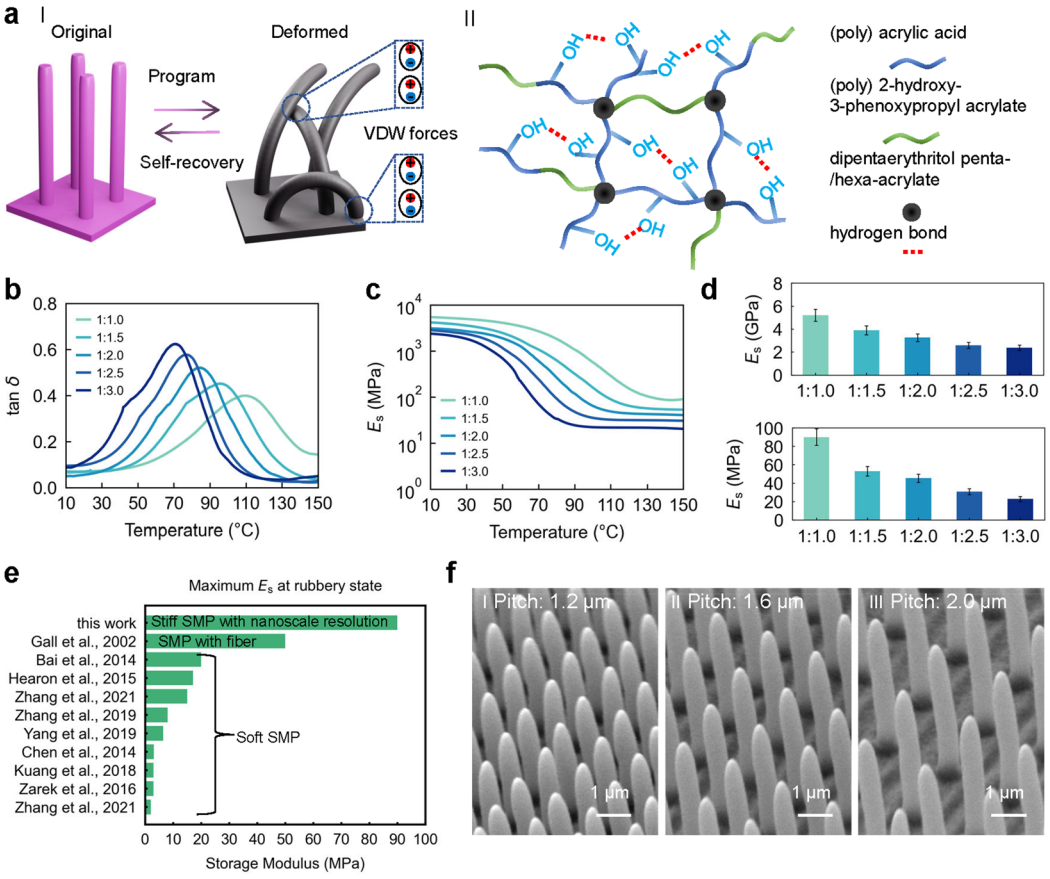

Figure 1. Design, characterization, and fabrication of nanostructures in stiff self-recovery materials. (a) (I) The concept of reconfigurable transformation of free-standing nanopillars. (II) Design of the acrylic acid (AAc) and 2-hydroxy-3-phenoxypropyl acrylate (HPPA) copolymer system. (b) Plot of tan δ (the ratio between loss modulus and storage modulus) as a function of temperature for different compositions (shown as the mass ratio between AAc and HPPA, with DPEPA kept at 0.8). (c) Storage modulus as a function of temperature for different compositions. (d) Storage modulus at room temperature (22 °C, top) and high temperature (40 °C above the glass transition temperature, bottom) for different compositions. Values in (d) represent the mean, and the error bars represent the standard deviation of the measured values (n = 3). (e) Comparison of the storage moduli of the SMPs in the rubbery state from different reported works (references in this panel are given in Table S1). (f) Tilted view (45°) scanning electron micrographs (SEM) of as-fabricated nanopillar arrays with varying pitches. Nanopillars have a nominal diameter of 400 nm and heights of 3.3, 3.9, and 3.9 μm respectively (aspect ratios of ∼8−10).

these tall and narrow structures can be deformed and stay in a collapsed and curled-up configuration yet remarkably overcome the VDW forces and recover when triggered by heat to achieve sub-micrometer-scale reconfigurable structures. High-resolution reconfigurable structural color prints and holograms are realized to demonstrate potential applications of the proposed materials.

For this study, we use the basic nanopillar geometry that has been shown to modulate the amplitude and phase of light at the single-pillar level.[33,34] The design principle is shown schematically in Figure 1aI. The fabricated nanopillars can be programmed into the deformed state, by applying stress at an elevated temperature where structures are in the rubbery state. After cooling down to the glassy state, the external stress can be removed, leaving structures in a deformed configuration. Reheating the structures above the glass transition temperature of the material recovers the nanopillars to their original state due to the shape memory effect,[35,36] overcoming the VDW forces between pillars in contact with each other or the substrate in the deformed state. A high storage modulus at the rubbery state is needed to enhance the restoring force and avoid lateral collapse of the pillar. Additionally, to achieve submicron resolution by TPL, the materials should polymerize fast upon light source exposure with a writing speed of ∼0.1 mm/s or higher to avoid overheating and bubbling caused by the high-energy femtosecond laser.

To meet these requirements, we designed a shape memory polymer resin based on a copolymer system of acrylic acid (AAc) and 2-hydroxy-3-phenoxypropyl acrylate (HPPA) (Figure 1aII). AAc is a shape memory monomer. It forms hydrogen bonds and offers high stiffness in the as-printed glassy state. Simultaneosly, it is a good solvent for polyvinylpyrrolidone (PVP), which was added to increase the viscosity of the resin to accelerate the printing speed[37] and enhance the support during the printing of freestanding structures[11] (see Methods in Part 1 in the Supporting Information). Poly HPPA functions as an elastomer at room temperature[38] and offers the flexibility needed to sustain large deformation in the set state of the pillars. The strong cross-linker dipentaerythritol penta-/hexaacrylate (DPEPA), containing multibranched acrylate functional groups (Figure S1), was adopted to impart the rigidity needed to overcome the VDW force during the recovery process and facilitate the polymerization process to pattern the polymer. To eliminate the influence of hydrogen bonds on the polymerized surface, a layer of (heptadecafluoro-1,1,2,2-tetrahydrodecyl)trimethoxysilane[39] was coated on the surface after fabrication (Methods in Part 1) to make it hydrophobic and decrease the surface energy.

https://doi.org/10.1021/acs.nanolett.2c03007
Nano Lett. XXXX, XXX, XXX−XXX

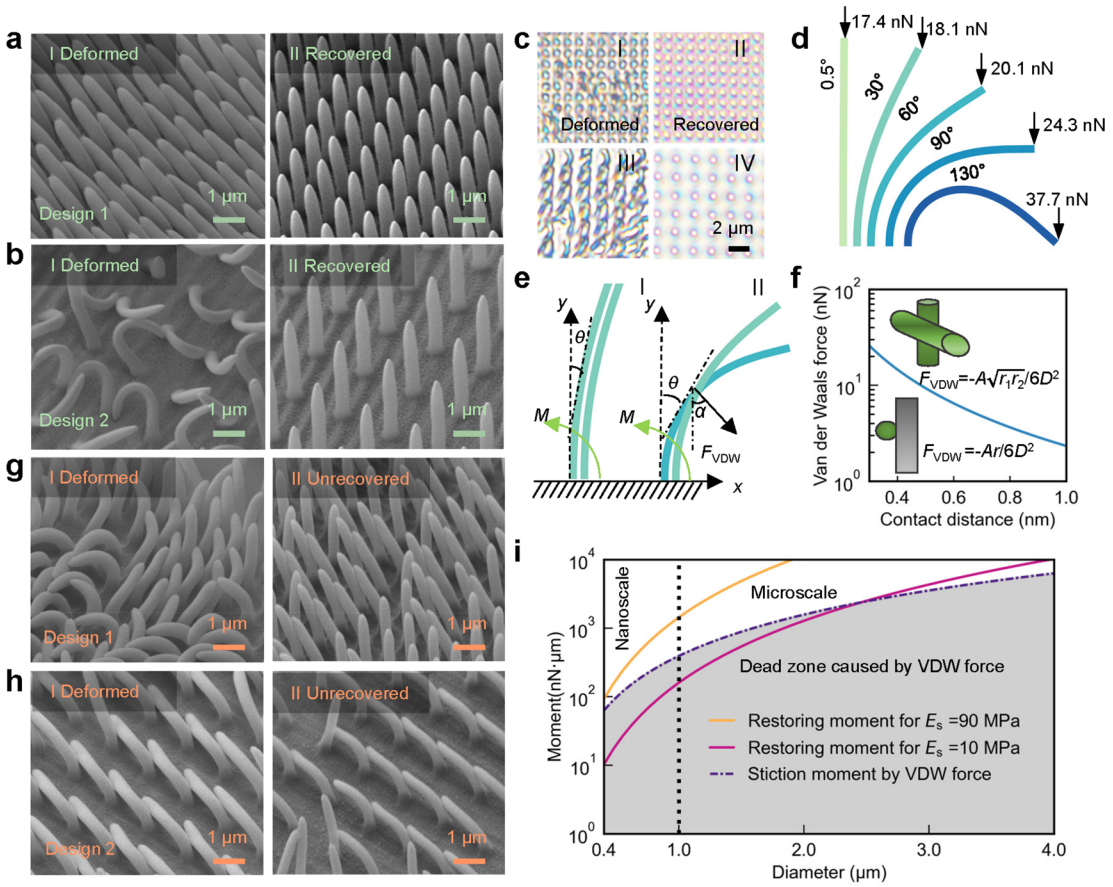

Figure 2. Study of recoverability of stiff vs soft nanopillars. (a, b) Tilted view (45°) SEM images of the deformed (I) and recovered (II) stiff nanopillars (E_s = 90 MPa) in dense (design 1, pitch 1.2 μm, aspect ratio ~8) and sparse arrays (design 2, pitch 2.0 μm, aspect ratio ~10). (c) Corresponding optical images of the deformed (I and III) and recovered (II and IV) nanopillars. (d) Calculated force to bend a nanopillar (diameter 400 nm, height 4 μm) to different angles and the corresponding bent shapes. (e) Force analysis of two nanopillars in the bent state for two separated (I) and touching (II) pillars. M represents the restoring moment of bent pillars, θ is the bending angle, and α is the direction of the VDW force F_{VDW}. (f) Calculated VDW force as a function of the contact distance for both crossed cylinders (upper inset) and sphere-wall (lower inset) cases. These two cases are equivalent if the two pillars and the pillar tip hemisphere have the same diameter. A is the Hamaker constant, r_1 and r_2 are the radii of the two pillars, r is the radius of the pillar tip, and D is the contact distance. (g, h) Tilted view (45°) SEM images of the deformed (I) and unrecovered (II) soft nanopillars (E_s = 10 MPa) for designs 1 and 2, respectively. (i) Calculated restoring moment and stiction moment by VDW force as a function of pillar diameter for a fixed aspect ratio of 8 and bending angle of 90° with VDW force acting on the tip of the pillar showing the dominance of VDW forces for structures with diameters smaller than ~2.2 μm for nanostructures in materials with a low storage modulus of 10 MPa. Increasing the storage modulus to 90 MPa enables sub-micrometer reconfigurable nanostructures as the restoring moment exceeds the VDW moment. The gray region represents the "dead zone" where pillars with a restoring moment in this region cannot recover.

The low peak values of the loss tangent tan δ (ratio between loss modulus and storage modulus) range from 0.40 to 0.61 (Figure 1b), indicating that the material effectively stores the strain energy, which can later be used to overcome VDW forces during the recovery stage. This material system thus exhibits a higher degree of elasticity above the glass transition temperature, in contrast to traditional SMPs with a peak tan δ value larger than 1. By adjusting the proportion of the chemical composition, a wide range (52−106 °C) of glass transition temperatures (T_g) (determined from the peak of tan δ) (Figure 1b) can be achieved. The storage modulus of the polymer increases with the increasing concentration of acrylic acid (Figure 1c). High storage moduli of ~2.4−5.2 GPa at 22 °C and ~22.7−90 MPa in the rubbery state were observed, as shown in Figure 1d. A mass ratio of 1:1:0.8 (AAc, HPPA, and DPEPA, respectively) was used in this work unless otherwise specified, with a storage modulus of 5.2 GPa at 22 °C and ~90 MPa at 150 °C in the rubbery state. This storage modulus in the rubbery state is almost 1 order of magnitude higher than those reported for soft SMPs and even ~2× higher than those of fiber-reinforced polymers (Figure 1e). Where necessary, the storage modulus can be further increased by increasing the ratio of cross-linker or decreasing the amount of elastomer. By preparing a photoresist based on this composition (methods) and patterning by TPL (Methods in Part 1 and Figure S2), nanopillars with aspect ratios of ~8−10 and pitches of 1.2−2.0 μm can be easily fabricated (Figure 1f). Here the aspect ratio is defined as the height divided by the diameter in the middle part of the nanopillar (Figure S3). The formulated polymer has a storage modulus as high as 5.2 GPa in the glassy state, benefiting from the acrylic acid monomer and strong cross-linker adopted, making it possible to print nanopillars with an aspect ratio as high as 10. This high storage modulus also contributes to the stability during the developing process after printing, where the high-aspect-ratio structures may collapse due to the capillary force[40] if traditional soft stimuli-responsive materials are used. In applications such as optics, the high aspect ratio can enhance the optical performance of the structures in several ways. For example, to get a green

https://doi.org/10.1021/acs.nanolett.2c03007
Nano Lett. XXXX, XXX, XXX−XXX

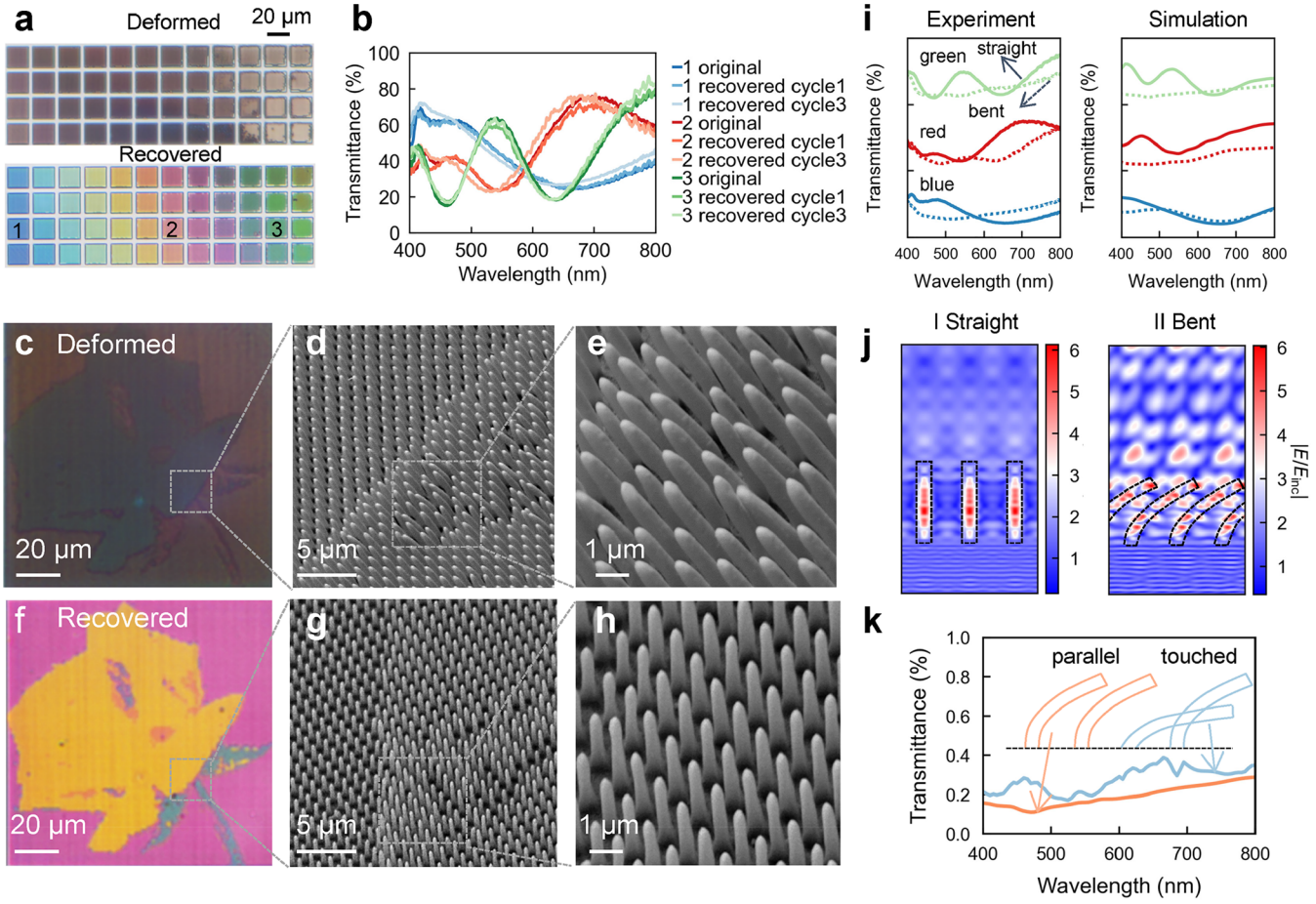

Figure 3. High-resolution reconfigurable structural color. (a) Optical images of deformed and recovered states of different structural colors. (b) Comparison of spectra of different colors (marked as 1−3 in (a)) at the original state and recovered states after different programming cycles. (c) Optical transmittance micrograph of a deformed color microprint consisting of nanopillars observed under an objective lens (NA = 0.2, CA = 11.5°). (d, e) Tilted view (45°) SEM images of the programmed painting. (f−h) Optical transmittance micrograph and corresponding tilted view (45°) SEM images of the recovered painting. (i) Measured and simulated transmittance spectra of blue, red, and green nanopillars at the straight (solid lines) and bent (dashed lines) states. (j) Cross-section views of the near-field normalized electric field amplitude at 550 nm wavelength for green nanopillars (at the straight and bent states, respectively). (k) FDTD simulation results for two bent nanopillars with parallel and touched configurations.

color by low-refractive-index (∼1.5) polymers, structures with aspect ratios of ∼7 are needed.[34] Also, to erase the phase information on the structures completely, high-aspec-ratio structures are preferred, as they can be deformed more heavily compared to low-aspect-ratio designs such as phase planes.[41,42]

To study the recoverability of the stiff material, we 3D-printed nanopillars in dense and sparse arrays, denoted as designs 1 and 2 with pitches of 1.2 and 2 μm, respectively. The nanopillars were programmed by compressing at 126 °C (20 °C above T_g) with a pressure of 100 psi using a Nanonex nanoimprint machine (Methods in Part 1 and Figure S4). In both designs, the pillars were bent in random directions, resulting in some pillars touching each other (Figure 2aI,bI). Cooling the nanostructures to room temperature with constant pressure applied stores them in the deformed state as the polymer chains remain kinetically trapped even after the stress is lifted. Heating the sample to 170 °C brings the pillars into the rubbery state again, triggering the distorted pillars to recover to their original standing state (Figure 2aII,bII). In this rubbery state, the stored energy is released and its restoring force exceeded the VDW force between the touching pillars. The structures of the same sample can be directly observed under an optical microscope before and after recovery (Figure 2c). The shape recovery process was completed within 60 s on heating above the glass transition temperature (Video 1 in the Supporting Information). Using classical elasticity theory, we calculated the forces acting at the tip of a single pillar to bend it to different angles and its corresponding bent shape (Figure 2d and Part 7 in the Supporting Information). These shapes agree with those observed in the SEMs of deformed nanopillars. During the self-recovery process, isolated pillars can recover freely due to the restoring moment M at the base and along the length of the pillar (Figure 2eI and eq S4 in the Supporting Information). When the pillars are touching, the restoring moment M needs to be larger than the moment caused by the VDW force between pillars (Figure 2eII). Thus, a higher storage modulus produces higher restoring moments, leading to nanostructure recovery.

We considered VDW forces in two commonly observed cases: between two nanopillars and between the tip of a nanopillar and the base of the print. Assuming that nanopillars have equal diameters, the VDW stiction force for both cases is the same as described in eq S5 in the Supporting Information and plotted versus contact distance as shown in Figure 2f. We then consider how the restraining stiction moment provided by the VDW force competes against the restoring moment of a soft pillar (storage modulus of 10 MPa) and a stiff pillar (storage modulus of 90

https://doi.org/10.1021/acs.nanolett.2c03007
Nano Lett. XXXX, XXX, XXX−XXX

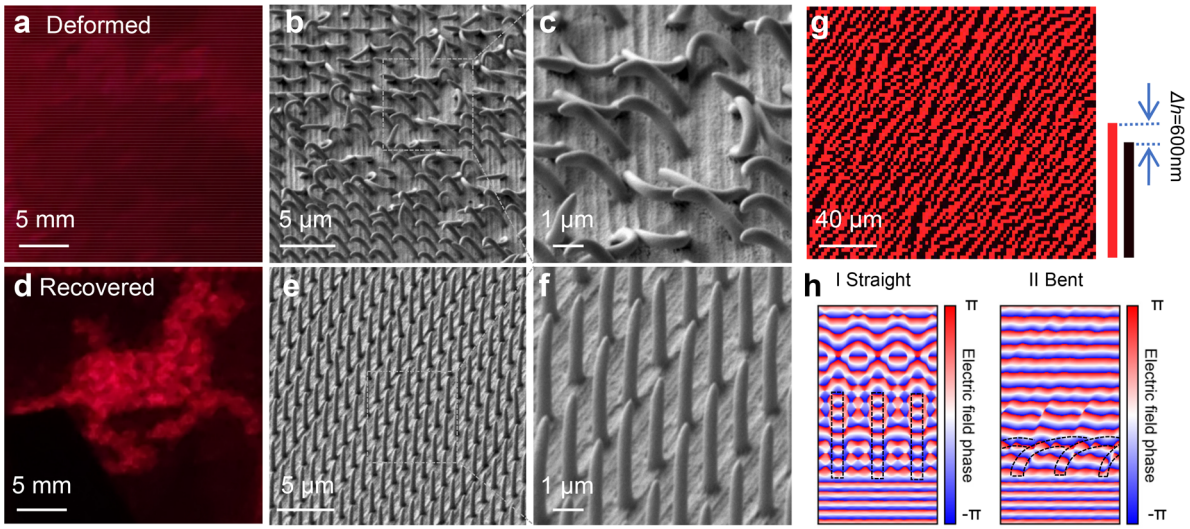

Figure 4. High-resolution reconfigurable hologram. (a) Far-field holographic projection from a sample of deformed nanopillars under 635 nm red laser illumination showing noise. (b, c) Tilted view (45°) SEM images of the deformed painting. (d–f) Projection and corresponding tilted view (45°) SEM images of a recovered hologram, respectively. (g) Binary phase map of the designed hologram. The red pixels represent phase π, and black pixels represent 0. The design consists of 100 × 70 pixels with each size of 2 × 2 μm^2. (h) Cross-sectional views of the near-field phase map at 635 nm wavelength for nanopillars in the straight and bent states.

MPa). The respective restraining and restoring moments were calculated for a 90° bending angle and contact distance of ∼0.3 nm[23] and plotted as a function of pillar diameter in Figure 2i (see Part 7 in the Supporting Information for calculations). At diameters smaller than ∼2.2 μm, the restoring moment for the soft pillar falls into the "dead zone" (gray region), where it is lower than the stiction moment. In contrast, the restoring moment of the stiff pillar is higher than the stiction moment for all pillar diameters down to 400 nm, which corresponds to the nominal diameter of nanopillars in this study. Note that nanopillars with lower bending angles have lower restoring moments. Our calculation shows that, for a bending angle as small as 20°, the stiff nanopillars can still recover, while the soft pillars cannot (Figure S5). Bending angles smaller than 20° were not considered as these nanopillars are unlikely to touch with each other.

A control experiment was conducted to examine the self-recovery effect of pillars made from the soft material (Part 8 in the Supporting Information). With the same design and fabrication process as in Figure 2a,b for the stiff pillars, the soft pillars that touched could no longer recover due to the stickiness caused by the VDW force (Figure 2g,h), indicating the advantage of the stiff material. Note that, for designs of other reversible geometries at the sub-micrometer scale, this effect of stiction will need to be considered. To examine this, we printed tall gratings instead of pillars (Figure S7) and observed a similar trend: i.e., the structures of a stiffer material can overcome the VDW stiction force where the softer counterpart remains permanently stuck. The shape recovery might depend on the pillar aspect ratio and pitch as seen in larger structures.[43] To investigate these two factors, pillars with different aspect ratios and pitches were fabricated and programmed. The degree of recovery remains at 100% for aspect ratios no larger than 8 for all pitches (Figure S8). Here, the recovery ratio was defined as $n_{recovered}/n_{total}$, where $n_{recovered}$ is the number of pillars recovered to the straight state and n_{total} is the total number of pillars per printing area (20 μm × 20 μm). A higher aspect ratio leads to partial recovery, especially along the edges of the printed area (insets of Figure S8), which may be caused by the stress concentration along the edges during the compression procedure. For a pitch of 1.2 μm, an aspect ratio larger than 10 was not examined because the pillars would collapse due to capillary forces during the development and drying process (Figure S9).

Due to the interaction of the nanopillars with visible light, these programmable nanopillars could exhibit interesting optical effects. Different structural colors[34] can be printed by changing the number of printing layers and exposure time (Figure S10). The structural colors at the deformed and recovered states are given in Figure 3a. A comparison of the spectra of different structural colors recovered from multiple programming cycles shows nearly full recovery compared to the original spectra (Figure 3b). An image of a flower was printed with a pixel size of 1.2 μm (Figure 3f) and a resolution of ∼21150 dots per inch (dpi). This pixel resolution is ∼8.3 times higher than that in our previous study on sub-micrometer-scale patterning of SMPs,[32] benefiting from the single nanopillar pixel adopted. As a single nanopillar[33] can generate a vivid structural color, the cross-talk between adjacent pixels is strongly suppressed. By the programming process, the as-printed structures can be programmed into a dark patch (Figure 3c), with the pillars bending and some parts touching each other (Figure 3d,e). Upon heating to the elevated temperature (170 °C), the print recovered to its original state to reveal an image (Figure 3f), with the bent and connected pillars returning to the straight as-printed state (Figure 3g,h).

We simulated the bending of the pillar using finite element analysis (FEA) (Methods in Part 1 and Figure S11) and used the resulting shapes in a finite difference time domain (FDTD) simulation to compute the transmittance spectra of the pillar under white light illumination. Both experimental measurements and FDTD simulations show that the spectra of blue, red, and green colors were "flattened" in the bent state (Figure 3i), leading to the gray appearance in Figure 3a,c. Near-field electric field amplitude at a wavelength of 550 nm shows a wave-guiding mode within the straight nanopillar with light illuminated

https://doi.org/10.1021/acs.nanolett.2c03007
Nano Lett. XXXX, XXX, XXX−XXX

vertically from the bottom (Figure 3jI), while complex interference patterns are observed within the nanopillar and air in the bent state (Figure 3jII), resulting in a weaker wavelength-selective effect, hence flattening the peaks in the spectra (Figure 3i). The overall dark appearance of bent nanopillars in Figure 3a,c is in stark contrast to the transparent appearance of the compressed mesh structures consisting of softer SMPs in the overly constrained configuration.[32] As the pillars are isolated structures that act also as weak waveguides, light scatters at the interface with the surrounding trapped air between bent pillars, causing a decreased transmittance. Note that, for simplicity, a parallel configuration was adopted for simulating the spectra in the bent state. A comparison of the parallel and touched configurations (Figure 3k) shows that they have similar spectra devoid of well-defined peaks and troughs. The tuning of light amplitude can be extended to the near-infrared (NIR) light range (Figure S12), using the continuous mode in TPL to achieve larger diameters of the nanopillars (Figure S13).

Apart from controlling the amplitude of light, the nanopillars also manipulate the phase of light. A binary hologram of a horse was designed using pillars with a height difference Δh to generate $\Delta\Phi = \pi$ phase difference at 635 nm wavelength (Figure 4d). Δh is determined by the formula[42] $\Delta h = \Delta\Phi\lambda/[2\pi(n-1)]$, where λ is the wavelength of the laser and n is the refractive index of the material at the target wavelength. The binary phase for a hologram is obtained by an adaptive Fourier-transform-based computer-generated hologram algorithm.[44] We employed the Gerchberg−Saxton algorithm[45] to get the optimized phase with the constraints that only 0 and π values are accepted. To increase the final diffraction efficiency of the hologram, the original image was designed to be centrosymmetric (Figure S14). For the developed material, $n \approx 1.49$ (Figure S15), and a $\Delta\Phi = \pi$ phase difference can be obtained by printing pillars with an ∼600 nm height difference. In the deformed state, the hologram cannot be seen (Figure 4a), indicating complete deformation of the entire area of the hologram (Figure 4b,c). Heating led to the recovery of the hologram (Figure 4d) with the pillars in the recovered state (Figure 4e,f). The simulated phase of a pillar indicates the erasure of the phase information caused by the nanopillar in the bent state (Figure 4h), leading to the disappearance of the hologram.

We developed stiff shape memory polymers for high-resolution reconfigurable nanophotonics. The formulated material system not only produces high-aspect-ratio structures that can recover from large deformation and collapse but also functions as a high-resolution resin enabling sub-micrometer 4D printing[8] of other complex geometries. Sub-micrometer isolated structures that would otherwise remain permanently deformed can now overcome VDW forces and exhibit reconfigurability. With sub-micrometer features, interactions with light in the visible spectrum become possible, as demonstrated by the structural colors produced with ∼21150 dpi resolution. By controlling the amplitude and phase of light in the upright and collapsed states, we achieved erasable-recoverable color prints and diffractive optical elements potentially useful as microscopic temperature recording labels. Future works may consider applications in the NIR range, including tunable infrared imaging[46,47] and radiative cooling,[48] while large-scale fabrication technologies such as nanoimprinting[49] and self-assembly[50] should be implemented. We believe that our approach here could benefit the further miniaturization of reconfigurable devices in various research fields.

■ ASSOCIATED CONTENT

Supporting Information

The Supporting Information is available free of charge at https://pubs.acs.org/doi/10.1021/acs.nanolett.2c03007.

Experimental and characterization details and additional figures and tables as described in the text (PDF)

Shape recovery process captured under a 10 × 0.2 NA microscope (MP4)

■ AUTHOR INFORMATION

Corresponding Authors

Hao Wang − *Engineering Product Development, Singapore University of Technology and Design, Singapore 487372, Singapore;* orcid.org/0000-0001-5388-6691; Email: whchn@live.cn

Joel K. W. Yang − *Engineering Product Development, Singapore University of Technology and Design, Singapore 487372, Singapore;* orcid.org/0000-0003-3301-1040; Email: joel_yang@sutd.edu.sg

Authors

Wang Zhang − *Engineering Product Development, Singapore University of Technology and Design, Singapore 487372, Singapore;* orcid.org/0000-0002-1563-8918

Alvin T. L. Tan − *Engineering Product Development, Singapore University of Technology and Design, Singapore 487372, Singapore*

Anupama Sargur Ranganath − *Engineering Product Development, Singapore University of Technology and Design, Singapore 487372, Singapore;* orcid.org/0000-0002-3695-5138

Biao Zhang − *Engineering Product Development, Singapore University of Technology and Design, Singapore 487372, Singapore*

Hongtao Wang − *Engineering Product Development, Singapore University of Technology and Design, Singapore 487372, Singapore;* orcid.org/0000-0001-9736-2208

John You En Chan − *Engineering Product Development, Singapore University of Technology and Design, Singapore 487372, Singapore;* orcid.org/0000-0001-8054-3360

Qifeng Ruan − *Engineering Product Development, Singapore University of Technology and Design, Singapore 487372, Singapore;* orcid.org/0000-0002-1592-9010

Hailong Liu − *Engineering Product Development, Singapore University of Technology and Design, Singapore 487372, Singapore*

Son Tung Ha − *Engineering Product Development, Singapore University of Technology and Design, Singapore 487372, Singapore;* orcid.org/0000-0002-5475-8365

Dong Wang − *Engineering Product Development, Singapore University of Technology and Design, Singapore 487372, Singapore;* orcid.org/0000-0002-8569-8713

Venkat K. Ravikumar − *Engineering Product Development, Singapore University of Technology and Design, Singapore 487372, Singapore*

Hong Yee Low − *Engineering Product Development, Singapore University of Technology and Design, Singapore 487372, Singapore;* orcid.org/0000-0003-2949-0763

Complete contact information is available at: https://pubs.acs.org/10.1021/acs.nanolett.2c03007

https://doi.org/10.1021/acs.nanolett.2c03007
Nano Lett. XXXX, XXX, XXX−XXX

Notes

The authors declare no competing financial interest.

■ ACKNOWLEDGMENTS

This research was supported by the National Research Foundation (NRF) Singapore, under its Competitive Research Programme award NRF-CRP20-2017-0004 and NRF Investigatorship Award NRF-NRFI06-2020-0005, as well as the MTC Programmatic Grant M21J9b0085.

■ REFERENCES

(1) Lu, Y.; Aimetti, A. A.; Langer, R.; Gu, Z. Bioresponsive materials. *Nat. Rev. Mater.* **2016**, *2* (1), 16075.
(2) Jones, M. R.; Seeman, N. C.; Mirkin, C. A. Programmable materials and the nature of the DNA bond. *Science* **2015**, *347* (6224), 1260901.
(3) Truby, R. L.; Lewis, J. A. Printing soft matter in three dimensions. *Nature* **2016**, *540* (7633), 371−378.
(4) Zhang, B.; Li, H.; Cheng, J.; Ye, H.; Sakhaei, A. H.; Yuan, C.; Rao, P.; Zhang, Y. F.; Chen, Z.; Wang, R.; He, X.; Liu, J.; Xiao, R.; Qu, S.; Ge, Q. Mechanically Robust and UV-Curable Shape-Memory Polymers for Digital Light Processing Based 4D Printing. *Adv. Mater.* **2021**, *33*, 2101298.
(5) Ge, Q.; Chen, Z.; Cheng, J.; Zhang, B.; Zhang, Y.-F.; Li, H.; He, X.; Yuan, C.; Liu, J.; Magdassi, S.; Qu, S. 3D printing of highly stretchable hydrogel with diverse UV curable polymers. *Sci. Adv.* **2021**, *7* (2), No. eaba4261.
(6) Zarek, M.; Layani, M.; Cooperstein, I.; Sachyani, E.; Cohn, D.; Magdassi, S. 3D printing of shape memory polymers for flexible electronic devices. *Adv. Mater.* **2016**, *28* (22), 4449−4454.
(7) Tan, Y. J.; Godaba, H.; Chen, G.; Tan, S. T. M.; Wan, G.; Li, G.; Lee, P. M.; Cai, Y.; Li, S.; Shepherd, R. F.; Ho, S. J.; Tee, B. C. K. A transparent, self-healing and high-κ dielectric for low-field-emission stretchable optoelectronics. *Nat. Mater.* **2020**, *19* (2), 182−188.
(8) Ge, Q.; Sakhaei, A. H.; Lee, H.; Dunn, C. K.; Fang, N. X.; Dunn, M. L. Multimaterial 4D printing with tailorable shape memory polymers. *Sci. Rep.* **2016**, *6*, 31110.
(9) Zhang, B.; Serjouei, A.; Zhang, Y.-F.; Wu, J.; Li, H.; Wang, D.; Low, H. Y.; Ge, Q. Dual-stage thermosetting photopolymers for advanced manufacturing. *Chem. Eng. J.* **2021**, *411*, 128466.
(10) Zhang, Y.-F.; Li, Z.; Li, H.; Li, H.; Xiong, Y.; Zhu, X.; Lan, H.; Ge, Q. Fractal-based stretchable circuits via electric-field-driven microscale 3D printing for localized heating of shape memory polymers in 4D printing. *ACS Appl. Mater. Interfaces* **2021**, *13* (35), 41414−41423.
(11) Jin, D.; Chen, Q.; Huang, T.-Y.; Huang, J.; Zhang, L.; Duan, H. Four-dimensional direct laser writing of reconfigurable compound micromachines. *Mater. Today* **2020**, *32*, 19−25.
(12) Gladman, A. S.; Matsumoto, E. A.; Nuzzo, R. G.; Mahadevan, L.; Lewis, J. A. Biomimetic 4D printing. *Nat. Mater.* **2016**, *15* (4), 413−418.
(13) Hippler, M.; Blasco, E.; Qu, J.; Tanaka, M.; Barner-Kowollik, C.; Wegener, M.; Bastmeyer, M. Controlling the shape of 3D microstructures by temperature and light. *Nat. Commun.* **2019**, *10*, 232.
(14) Zeng, H.; Wasylczyk, P.; Parmeggiani, C.; Martella, D.; Burresi, M.; Wiersma, D. S. Light-fueled microscopic walkers. *Adv. Mater.* **2015**, *27* (26), 3883−3887.
(15) Zeng, H.; Zhang, H.; Ikkala, O.; Priimagi, A. Associative learning by classical conditioning in liquid crystal network actuators. *Matter* **2020**, *2* (1), 194−206.
(16) Ford, M. J.; Ambulo, C. P.; Kent, T. A.; Markvicka, E. J.; Pan, C.; Malen, J.; Ware, T. H.; Majidi, C. A multifunctional shape-morphing elastomer with liquid metal inclusions. *Proc. Natl. Acad. Sci. U.S.A.* **2019**, *116* (43), 21438−21444.
(17) Ze, Q.; Kuang, X.; Wu, S.; Wong, J.; Montgomery, S. M.; Zhang, R.; Kovitz, J. M.; Yang, F.; Qi, H. J.; Zhao, R. Magnetic shape memory polymers with integrated multifunctional shape manipulation. *Adv. Mater.* **2020**, *32* (4), 1906657.
(18) Chen, Z.; Zhao, D.; Liu, B.; Nian, G.; Li, X.; Yin, J.; Qu, S.; Yang, W. 3D printing of multifunctional hydrogels. *Adv. Funct. Mater.* **2019**, *29* (20), 1900971.
(19) Koenderink, A. F.; Alu, A.; Polman, A. Nanophotonics: Shrinking light-based technology. *Science* **2015**, *348* (6234), 516−521.
(20) Guo, L.; Jackman, J. A.; Yang, H.-H.; Chen, P.; Cho, N.-J.; Kim, D.-H. Strategies for enhancing the sensitivity of plasmonic nanosensors. *Nano Today* **2015**, *10* (2), 213−239.
(21) Lao, Z.; Sun, R.; Jin, D.; Ren, Z.; Xin, C.; Zhang, Y.; Jiang, S.; Zhang, Y.; Zhang, L. Encryption/decryption and microtarget capturing by pH-driven Janus microstructures fabricated by the same femtosecond laser printing parameters. *Int. J. Extreme Manuf.* **2021**, *3* (2), 025001.
(22) Zeng, H.; Wasylczyk, P.; Wiersma, D. S.; Priimagi, A. Light robots: bridging the gap between microrobotics and photomechanics in soft materials. *Adv. Mater.* **2018**, *30* (24), 1703554.
(23) Autumn, K.; Liang, Y. A.; Hsieh, S. T.; Zesch, W.; Chan, W. P.; Kenny, T. W.; Fearing, R.; Full, R. J. Adhesive force of a single gecko foot-hair. *Nature* **2000**, *405* (6787), 681−685.
(24) Duan, H.; Berggren, K. K. Directed self-assembly at the 10 nm scale by using capillary force-induced nanocohesion. *Nano Lett.* **2010**, *10* (9), 3710−3716.
(25) Li, S.; Deng, B.; Grinthal, A.; Schneider-Yamamura, A.; Kang, J.; Martens, R. S.; Zhang, C. T.; Li, J.; Yu, S.; Bertoldi, K.; Aizenberg, J. Liquid-induced topological transformations of cellular microstructures. *Nature* **2021**, *592* (7854), 386−391.
(26) Duan, H.; Yang, J. K.; Berggren, K. K. Controlled collapse of high-aspect-ratio nanostructures. *Small* **2011**, *7* (18), 2661−2668.
(27) Xia, X.; Afshar, A.; Yang, H.; Portela, C. M.; Kochmann, D. M.; Di Leo, C. V.; Greer, J. R. Electrochemically reconfigurable architected materials. *Nature* **2019**, *573* (7773), 205−213.
(28) Zhang, M.; Shahsavan, H.; Guo, Y.; Pena-Francesch, A.; Zhang, Y.; Sitti, M. Liquid-Crystal-Elastomer-Actuated Reconfigurable Microscale Kirigami Metastructures. *Adv. Mater.* **2021**, *33* (25), 2008605.
(29) Yang, C.; Boorugu, M.; Dopp, A.; Ren, J.; Martin, R.; Han, D.; Choi, W.; Lee, H. 4D printing reconfigurable, deployable and mechanically tunable metamaterials. *Mater. Horiz.* **2019**, *6* (6), 1244−1250.
(30) Wei, Y.-L.; Yang, Q.-S.; Ma, L.-H.; Tao, R.; Shang, J.-J. Design and analysis of 2D/3D negative hydration expansion Metamaterial driven by hydrogel. *Materials & Design* **2020**, *196*, 109084.
(31) Yuan, C.; Wang, F.; Ge, Q. Multimaterial direct 4D printing of high stiffness structures with large bending curvature. *Extreme Mech. Lett.* **2021**, *42*, 101122.
(32) Zhang, W.; Wang, H.; Wang, H.; Chan, J. Y. E.; Liu, H.; Zhang, B.; Zhang, Y.-F.; Agarwal, K.; Yang, X.; Ranganath, A. S.; Low, H. Y.; Ge, Q.; Yang, J. K. W. Structural multi-colour invisible inks with submicron 4D printing of shape memory polymers. *Nat. Commun.* **2021**, *12*, 112.
(33) Chan, J. Y. E.; Ruan, Q.; Jiang, M.; Wang, H.; Wang, H.; Zhang, W.; Qiu, C.-W.; Yang, J. K. W. High-resolution light field prints by nanoscale 3D printing. *Nat. Commun.* **2021**, *12*, 3728.
(34) Wang, H.; Ruan, Q.; Wang, H.; Rezaei, S. D.; Lim, K. T.; Liu, H.; Zhang, W.; Trisno, J.; Chan, J. Y. E.; Yang, J. K. Full color and grayscale painting with 3D printed low-index nanopillars. *Nano Lett.* **2021**, *21* (11), 4721−4729.
(35) Xie, T. Tunable polymer multi-shape memory effect. *Nature* **2010**, *464* (7286), 267−270.
(36) Jin, B.; Song, H.; Jiang, R.; Song, J.; Zhao, Q.; Xie, T. Programming a crystalline shape memory polymer network with thermo-and photo-reversible bonds toward a single-component soft robot. *Sci. Adv.* **2018**, *4* (1), No. eaao3865.
(37) Zandrini, T.; Liaros, N.; Jiang, L.; Lu, Y.; Fourkas, J.; Osellame, R.; Baldacchini, T. Effect of the resin viscosity on the writing properties of two-photon polymerization. *Optical Materials Express* **2019**, *9* (6), 2601−2616.
(38) Zhang, B.; Kowsari, K.; Serjouei, A.; Dunn, M. L.; Ge, Q. Reprocessable thermosets for sustainable three-dimensional printing. *Nat. Commun.* **2018**, *9*, 1831.

https://doi.org/10.1021/acs.nanolett.2c03007
Nano Lett. XXXX, XXX, XXX−XXX

(39) Ohnishi, S.; Yaminsky, V. V.; Christenson, H. K. Measurements of the force between fluorocarbon monolayer surfaces in air and water. *Langmuir* **2000**, *16* (22), 8360−8367.
(40) Lao, Z.; Zheng, Y.; Dai, Y.; Hu, Y.; Ni, J.; Ji, S.; Cai, Z.; Smith, Z. J.; Li, J.; Zhang, L.; et al. Nanogap Plasmonic Structures Fabricated by Switchable Capillary-Force Driven Self-Assembly for Localized Sensing of Anticancer Medicines with Microfluidic SERS. *Adv. Funct. Mater.* **2020**, *30* (15), 1909467.
(41) Lim, K. T.; Liu, H.; Liu, Y.; Yang, J. K. Holographic colour prints for enhanced optical security by combined phase and amplitude control. *Nat. Commun.* **2019**, *10*, 25.
(42) Wang, H.; Wang, H.; Zhang, W.; Yang, J. K. Toward near-perfect diffractive optical elements via nanoscale 3D printing. *ACS Nano* **2020**, *14* (8), 10452−10461.
(43) Chen, C. M.; Yang, S. Directed water shedding on high-aspect-ratio shape memory polymer micropillar arrays. *Adv. Mater.* **2014**, *26* (8), 1283−1288.
(44) Gerchberg, R. W. A practical algorithm for the determination of plane from image and diffraction pictures. *Optik* **1972**, *35* (2), 237−246.
(45) Wang, H.; Liu, Y.; Ruan, Q.; Liu, H.; Ng, R. J.; Tan, Y. S.; Wang, H.; Li, Y.; Qiu, C. W.; Yang, J. K. Off-Axis holography with uniform illumination via 3D printed diffractive optical elements. *Adv. Opt. Mater.* **2019**, *7* (12), 1900068.
(46) Tang, X.; Ackerman, M. M.; Chen, M.; Guyot-Sionnest, P. Dual-band infrared imaging using stacked colloidal quantum dot photodiodes. *Nat. Photonics* **2019**, *13* (4), 277−282.
(47) Ran, W.; Wang, L.; Zhao, S.; Wang, D.; Yin, R.; Lou, Z.; Shen, G. An integrated flexible all-nanowire infrared sensing system with record photosensitivity. *Adv. Mater.* **2020**, *32* (16), 1908419.
(48) Shi, N. N.; Tsai, C.-C.; Camino, F.; Bernard, G. D.; Yu, N.; Wehner, R. Keeping cool: Enhanced optical reflection and radiative heat dissipation in Saharan silver ants. *Science* **2015**, *349* (6245), 298−301.
(49) Cox, L. M.; Martinez, A. M.; Blevins, A. K.; Sowan, N.; Ding, Y.; Bowman, C. N. Nanoimprint lithography: Emergent materials and methods of actuation. *Nano Today* **2020**, *31*, 100838.
(50) Cummins, C.; Lundy, R.; Walsh, J. J.; Ponsinet, V.; Fleury, G.; Morris, M. A. Enabling future nanomanufacturing through block copolymer self-assembly: A review. *Nano Today* **2020**, *35*, 100936.

https://doi.org/10.1021/acs.nanolett.2c03007
Nano Lett. XXXX, XXX, XXX−XXX